Applied Thermal Engineering 62 (2014) 141–147

Contents lists available at ScienceDirect

Applied Thermal Engineering

journal homepage: www.elsevier.com/locate/apthermeng

Effect of Mach number on thermoelectric performance of SiC ceramics nose-tip for supersonic vehicles

Xiao-Yi Han [a,b,*], Jun Wang [a]

[a] Science and Technology on Advanced Ceramic Fibers and Composites Laboratory, College of Aerospace Science and Engineering, National University of Defense Technology, Changsha 410073, PR China
[b] Engineering Design Institution of Nanjing Military Command, Nanjing 210016, PR China

HIGHLIGHTS

- Thermoelectric SiC nose-tip structure for aerodynamic heat harvesting of high-speed vehicles is studied.
- Thermoelectric performance is predicted based on numerical methods and experimental thermoelectric parameters.
- The effects of Mach number on thermoelectric performance are studied in the present paper.
- Results with respect to the Thomson effect are also explored.
- Output power and energy efficiency of the thermoelectric nose-tip are increased with the increase of Mach number.

ARTICLE INFO

Article history:
Received 21 April 2013
Accepted 6 September 2013
Available online 25 September 2013

Keywords:
Thermoelectric energy efficiency
Silicon carbide
Supersonic vehicles
Thomson heat

ABSTRACT

This paper focus on the effects of Mach number on thermoelectric energy conversion for the limitation of aero-heating and the feasibility of energy harvesting on supersonic vehicles. A model of nose-tip structure constructed with SiC ceramics is developed to numerically study the thermoelectric performance in a supersonic flow field by employing the computational fluid dynamics and the thermal conduction theory. Results are given in the cases of different Mach numbers. Moreover, the thermoelectric performance in each case is predicted with and without Thomson heat, respectively. Due to the increase of Mach number, both the temperature difference and the conductive heat flux between the hot side and the cold side of nose tip are increased. This results in the growth of the thermoelectric power generated and the energy conversion efficiency. With respect to the Thomson effect, over 50% of total power generated converts to Thomson heat, which greatly reduces the thermoelectric power and efficiency. However, whether the Thomson effect is considered or not, with the Mach number increasing from 2.5 to 4.5, the thermoelectric performance can be effectively improved.

1. Introduction

When cruising in atmosphere, supersonic vehicles are confronted with high thermal loads on leading-edges. There have been many efficient heat dissipation mechanisms for preventing extremely dangerous damage to the geometry configuration of vehicles from serious aero-heating, such as blunted waverider [1], film cooling [2], heat-pipe cooling [3], transpiration cooling [4] and opposing jet cooling [5]. However, the dispersed aerodynamic heat is hardly reusable and recycled.

Recently, a feasible application was proposed for the supersonic vehicles aiming at converting aero-heating quantity to electricity by thermal photovoltaic system (TPV) [6]. TPV is a kind of thermoelectric energy conversion technique, which enables heat-electricity direct conversion. Instead of dispersing most of aerodynamic heat, the thermoelectric technology enables the energy harvesting from it. Thermoelectric technology is very promising in low level thermal energy recovery. Jang and Tsai [7] studied the optimization of thermoelectric modules attached to the chimney plate for waste gas heat recovery. Kim et al. [8] designed a new thermoelectric generation system with enlarged hot surface area for heat pipes. Nuwayhid et al. [9] used commercial available thermoelectric modules to evaluate the feasibility of stove-run thermoelectric generators for domestic electricity supply. Min and Rowe [10] developed a thermoelectric system with combusted

* Corresponding author. Science and Technology on Advanced Ceramic Fibers and Composites Laboratory, College of Aerospace Science and Engineering, National University of Defense Technology, Changsha 410073, PR China.
E-mail address: dolcehan@gmail.com (X.-Y. Han).

1359-4311/$ – see front matter © 2013 Elsevier Ltd. All rights reserved.
http://dx.doi.org/10.1016/j.applthermaleng.2013.09.011

Nomenclature

Alphabetization

A	area (cm^2)
E_i, F_i, G_i	inviscid terms for flow
E_v, F_v, G_v	viscous terms for flow
I	current (A)
M	Mach number
P	output power (W)
P_{Th}	power excluding Thomson heat (W)
p	pressure (kPa)
Q	heat transfer rate (W)
Q_{Th}	Thomson heat rate (W)
R	electric resistance (Ω)
S	source terms for flow
St	Stanton number
T	absolute temperature (K)
ΔT	temperature difference (K)
t	time (s)
U	conservation variable
V	thermoelectric voltage (mV)
x, y, z	cartesian coordinates

Greek symbols

α	Seebeck coefficient (V/K)
η	energy conversion efficiency (%)
κ	thermal conductivity (W/(m K))
π	Peltier coefficient (m)
ρ	electric resistivity (Ω mm)
Φ	heat flux rate (W)

Subscripts

C	cold side
H	hot side
L	Load
∞	free stream static

Abbreviations

N–S	Navier–Stokes
SST	shear stress transport

heat as its thermal input. It is widely recognized that the thermoelectric equipment and devices are reliable, safe and capable to generate a minimum acceptable power, and have been found very extensive applications in specific areas, such as military and aerospace [11]. As sunshine and other light sources most needed for the photovoltaic units may not be available in the cabin, the use of TPV may not be as efficient as expected. Since the main feature of the temperature distribution on supersonic vehicles leading-edges is the large temperature difference rather than the multiple thermal sources provided, it is more feasible to use structural materials with thermoelectric function [12].

SiC matrix ceramics [13] and SiC-based composites [14] are high-temperature structural materials widely applied in space vehicles. Besides, SiC ceramics perform good thermoelectric properties at high temperatures [15], and can be applied to chip cooling [16]. Even though the thermoelectric figure of merits of SiC ceramics is relatively low, it can be greatly improved by several approaches, for example, doping [17]. So far, the prospect of SiC materials in thermoelectric applications is notable for their thermal stability and high specific strength in large temperature range. In this work, a nose-tip model constructed with SiC ceramics is developed to predict the thermoelectric energy conversion performance in a supersonic flow field by computational fluid dynamics and thermal conduction theory. The effect of Mach number on the thermoelectric performance is discussed in detailed.

2. Materials and methods

2.1. Nose-tip model and numerical methods

As shown in Fig. 1, the nose-tip model is 40.6 mm in length, and has a hemisphere-shaped leading edge, which is 25.5 mm in diameter. The flow field parameters and heat fluxes were obtained by solving three-dimensional N–S governing equations with the SST turbulence model [18,19]. The steady-state full N–S equations in conservation form are given by

$$\frac{\partial \boldsymbol{U}}{\partial t}+\frac{\partial \boldsymbol{E}_i}{\partial x}+\frac{\partial \boldsymbol{F}_i}{\partial y}+\frac{\partial \boldsymbol{G}_i}{\partial z}=\frac{\partial \boldsymbol{E}_v}{\partial x}+\frac{\partial \boldsymbol{F}_v}{\partial y}+\frac{\partial \boldsymbol{G}_v}{\partial z}+\boldsymbol{S} \tag{1}$$

Because no chemical reactions are involved, S is set to zero. The convective terms are approximated using the Van-leer flux splitting method [20], and the viscous terms using the central difference method. A semi-explicit Runge–Kutta scheme is used for the time integration [21]. The temperature distributions of the flow field and solid nose-tip model are obtained by solving heat conduction equation [22]. The grids of the simulation model in the symmetrical plane, outlet and the surface of the nose-tip are shown in Fig. 2. The boundary conditions are listed in Table 1. It is assumed that the fluid–solid interface is no-slip and the nose-tip solid region is unexpanded and undistorted. The radius heat transfer in solid region is ignored, because the maximum temperature is nearly 1000 K, below which the radius heat is relatively small.

2.2. Evaluation of thermoelectric performance

In an effective circuit shown in Fig. 3, the nose-tip structure serves as the thermoelectric module. Only the thermoelectric properties of the nose-tip materials (SiC) are considered to study specially the recovery capability of model. When temperature difference applying on the nose-tip, the generated open circuit voltage is given by

$$V = \pi_H - \pi_C \tag{2}$$

Assuming constant thermal conductivity and internal electric resistance of nose-tip, the rates of supply heat flux at the hot side and removal heat flux at the cold side are expressed as

$$\Phi_H = \pi_H I - Q - 0.5 I^2 R \tag{3}$$

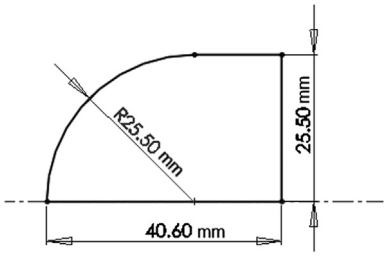

Fig. 1. Scheme of the nose-tip model (in mm).

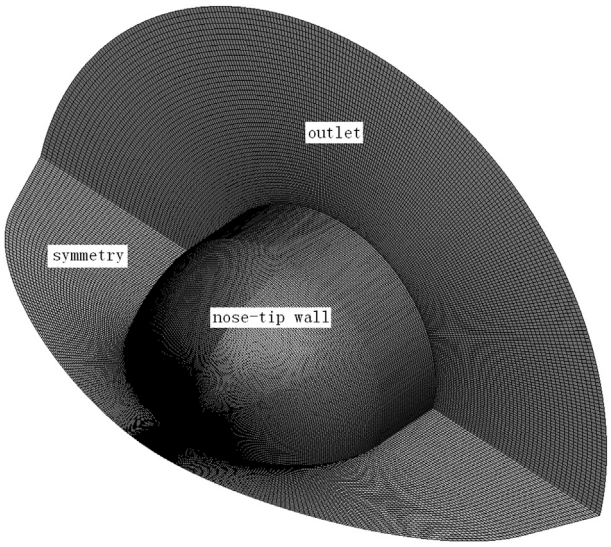

Fig. 2. Grids on the simulation model.

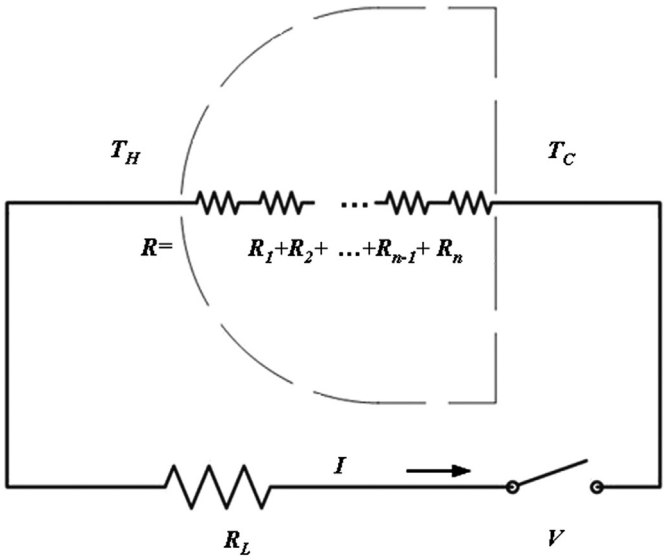

Fig. 3. Schematic diagram of nose-tip thermoelectric module.

$$\Phi_C = \pi_C I - Q + 0.5I^2R \tag{4}$$

of which the items on the right side in turn are Peltier heat, conductive heat, and Joule heat. Instead of the actual value, the average internal electric resistance is expressed as

$$R_{(T_C,T_H)} = \int_{T_C}^{T_H} R(T)\mathrm{d}T/(T_H - T_C) \tag{5}$$

The generated power can be calculated by either multiplying output current with loaded electric resistance or the variation of heat flux as follows:

$$P = I^2R_L = V^2R_L/(R+R_L)^2 = \Phi_H - \Phi_C \tag{6}$$

The thermoelectric energy conversion efficiency of nose-tip model is given by

$$\eta = P/\Phi_H \tag{7}$$

Thomson heat relates to the rate of generation of reversible heat with results from the passage of a current along a portion of a single conductor along which there is a temperature difference ΔT. Although the Thomson heat is not of primary importance in thermoelectric devices, it must be considered in detailed calculations [23,24]. Thomson heat and the output power are illustrated by

$$Q_{Th} = (\mathrm{d}\pi_H/\mathrm{d}T - \mathrm{d}\pi_C/\mathrm{d}T)I\Delta T \tag{8}$$

$$P_{Th} = (\pi_H - \pi_C)I - Q_{Th} - I^2R \tag{9}$$

Accordingly, the energy efficiency considering Thomson effect is expressed as

Table 1
Computational boundary conditions of flow field and nose region.

Item	Value
Free stream Mach number, M	2.5–4.5
Free stream static pressure, p_∞	5.475 kPa
Free stream static temperature, T_∞	217 K
Cold side temperature of prototype, T_C	300 K

$$\eta_{Th} = P_{Th}/\Phi_H \tag{10}$$

2.3. Thermoelectric properties of the SiC materials

Series of SiC ceramics and composites have been investigated on their thermoelectric properties. However, there are few comprehensive reports on the thermoelectric parameters of polymer-derived SiC materials applied for aerospace structures, such as thermal conductivity, electric resistivity and Seebeck coefficient. In order to obtain the needed parameters, dense SiC ceramics were prepared with the preceramic precursor polycarbosilane produced by our laboratory [25]. The Peltier coefficient and electric conductivity were measured by four-probe method (ZEM-3, ULVAC-RIKO, Japan). The thermal conductivity was studied using laser-flashed method (LFA457, Netzsch, Germany). Archimedes method was used to measure the density of the consolidated SiC sample with deionized water as the immersion medium.

The measured density of the consolidated SiC sample is 1.72 g/cm^3. Since the thermal conductivity varies very slightly in the temperature range of 300 K–923 K, it is assumed to be constant, and its average value is 5.73 W/(m K). Peltier coefficient (π) and electric resistivity (ρ) versus temperatures of the SiC ceramics are

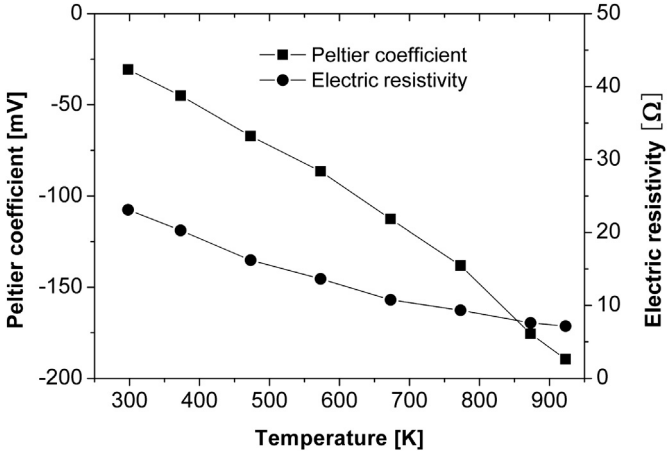

Fig. 4. Peltier coefficient and electric resistivity of the dense SiC ceramic materials.

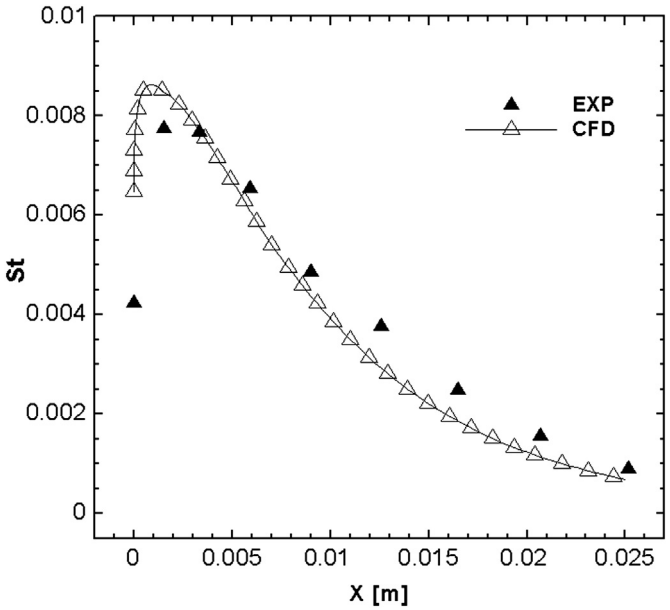

Fig. 5. Experimental and numerical Stanton number along nose-tip surface comparison.

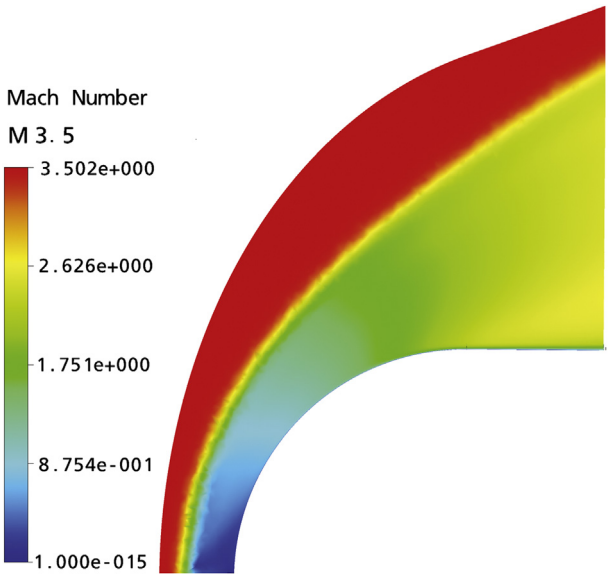

Fig. 6. Mach number distribution in the flow field (symmetrical plane, M 3.5).

shown in Fig. 4. With the elevated temperature, the absolute value of π increases, and inversely, ρ decreases. Results suggest good thermoelectric properties of SiC at even higher temperatures.

3. Validation of computational methods

Prior to computation, a verification of the algorithm and grid independence of the numerical solution is performed to ensure the accuracy and validity of the results. Flow conditions is chosen according to the related experiment in Ref. [26]. As shown in Fig. 5, the predicted Stanton numbers (St) along the surface of the hemisphere nose are compared with the experimental data. The numerical and experimental results are in good agreement with each other. There are nine experimental data points, except the first one, the simulation accuracies of the remaining points are in 15%, of which the best one is close to 1%. The discrepancy is attributed to the computation error, assumption of the simulation model and experimental measurement error. Especially with the stagnation point, the discrepancy is much bigger for two main reasons. For one thing, due to a significant temperature gradient around the stagnation, a little change of position will cause a large variety of the heat flux; for the other, it is hard to measure the heat flux accurately in the stagnation region.

4. Results and discussion

By means of above numerical procedures, the flow parameters and the thermal conditions can be obtained. The Mach number distribution in flow field (M 3.5) is shown in Fig. 6. And the temperature distributions of the flow field and nose tip are given in Figs. 7 and 8, respectively. The highest temperature of the supersonic flow is over 746 K, and the temperature at the stagnation of the nose-tip region is up to 655 K. With the temperature at the cold side of the nose model set to 300 K, as a result, a temperature difference between the two sides of 355 K is obtained.

Both the temperature difference ΔT between the hot and the cold surfaces and the conductive heat flux Q increase as the Mach number increases. As shown in Fig. 9, at M 4.5, the temperature difference reaches as high as 670 K, nearly seven times of that at M 2.5. And the heat flux density is nearly four times of that at M 2.5. On the other hand, the internal electric resistance decreases, while the thermoelectric voltage of the nose-tip model increases with the increase of Mach number, as shown in Fig. 10. The thermoelectric voltage is about 0.175 mV at M 4.5, and the electric resistance of the nose model reduces to nearly 0.12 Ω. Results indicate better thermoelectric performance at high Mach numbers.

The performance of the thermoelectric nose tip can be characterized. Under the conditions of different Mach numbers, the generated output power and the energy efficiency as a function of current neglecting Thomson effect are illustrated in Fig. 11. From M 2.5 to M 4.5, the maximum current increases from 0.12 A to 1.44 A. Larger current is permitted at higher Mach numbers, in which case the circuit has larger thermoelectric voltage and smaller internal electric resistance. When the loaded electric resistance of the circuit equals to the internal electric resistance of the nose-tip, the maximum power and maximum efficiency is obtained. As shown in

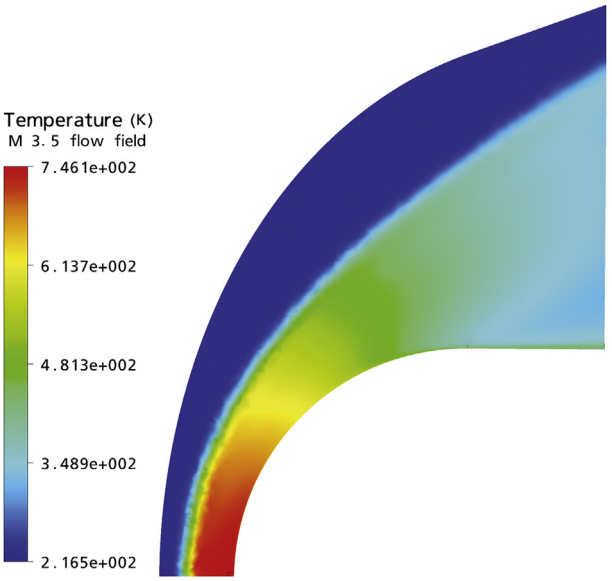

Fig. 7. Temperature distribution in the flow field (symmetrical plane, M 3.5).

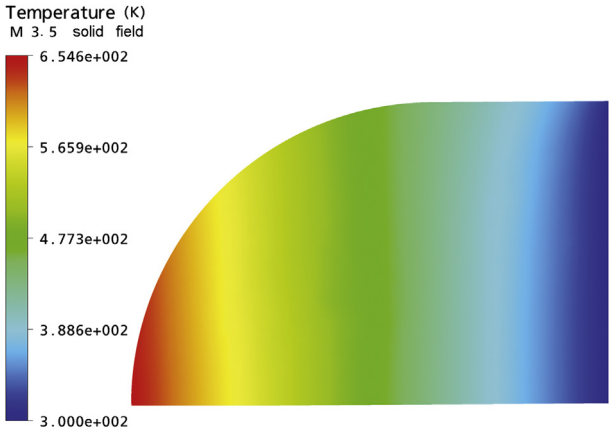

Fig. 8. Temperature distribution in the nose-tip region (symmetrical plane, M 3.5).

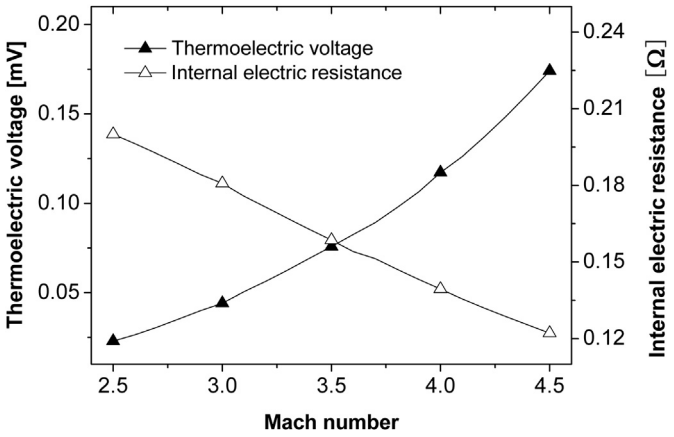

Fig. 10. Thermoelectric voltage and internal electric resistance of nose-tip at different Mach numbers.

Fig. 12, both the maximum of output power and energy efficiency are increased with the elevated Mach numbers attributed to enlarged temperature difference, heat flux, thermoelectric voltage, and the decrease of internal electric resistance (also see Figs. 9 and 10). The maximum of power output at M 4.5 is over 0.062 W, 30 times larger than that of M 2.5. That is almost 0.25 W/cm^2 on average (divided by the cold side area, about 0.204 cm^2). Correspondingly, the maximum energy efficiency increased with the increase of Mach number. At M 4.5 the maximum efficiency is 0.22%, about 10 times of that at M 2.5.

Thomson heat would grow much faster if there were large temperature difference or exceeding circuit current. Under the condition of each Mach number, the output power reduces to less than a half of the total generated power. As shown in Fig. 13, at M 4.5 the output power is 0.021 W, which possesses less than 30% of the generated thermoelectric power. The energy conversion efficiency also decreases dramatically. The maximum value reduces to 0.0085% at M 4.5, less than a half of the one without respect to the Thomson effect (0.022%). It is also observed that the maximum current is reduced with respect to the Thomson effect. This is because partial generated power transfers to Thomson heat, and relatively smaller electric power is remained.

Although higher Mach number results in much greater Thomson heat, the thermoelectric performance will be improved due to the continuously increasing thermoelectric voltage and decreasing electric resistance of the nose-tip. In order to maintain thermoelectric voltage large enough, the absolute value of Seebeck coefficient (α) should be enlarged. On the other hand, according to (8), of which the Peltier coefficient is related to Seebeck coefficient α by Kelvin relations:

$$\alpha \cong \pi / T \tag{11}$$

the Seebeck coefficient should remain constant in a wide range of temperature in order to eliminate the effect of Thomson heat. It is well recognized that nanostructured materials, such as superlattices, quantum dots, nanowires, and nanocomposites play a role in optimizing the Seebeck coefficient [27]. For this reason, the application of the thermoelectric nose-tip for aerospace vehicles at high Mach numbers is encouraging.

It is notable that the thermal conductivity and electric resistance are assumed constant at each case, and that the thermoelectric generated model is reduced to one dimensional problem. The computational results may not be in good agreement with the real ones. With further studies the three-dimensional numerical model

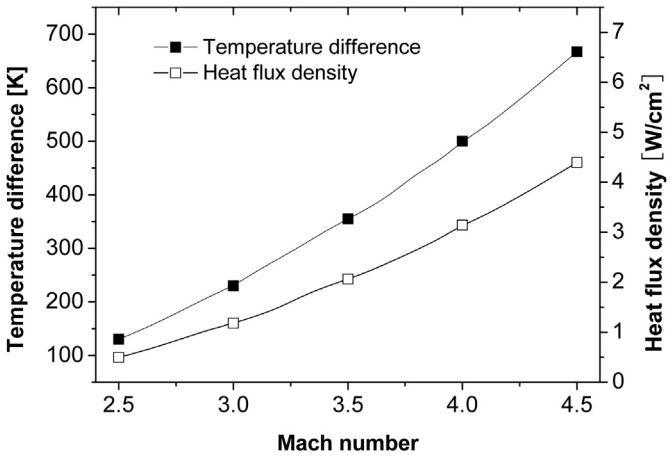

Fig. 9. Temperature difference between the hot and cold side and conductive heat flux density at different Mach numbers.

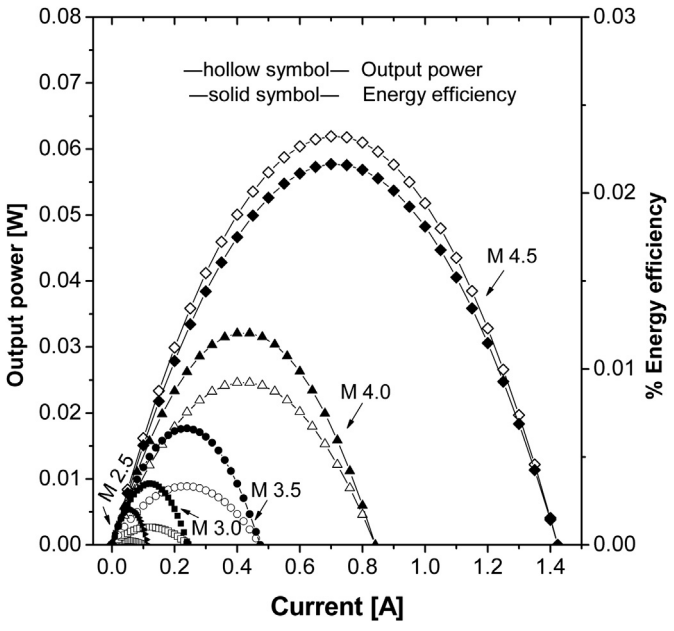

Fig. 11. Output power and energy efficiency of nose-tip versus current at different Mach numbers.

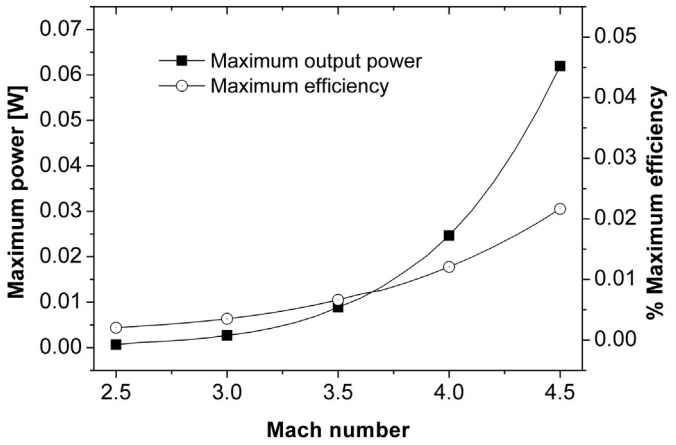

Fig. 12. Maximum of output power and energy efficiency at different Mach numbers.

introduced, the results will be more accurate. Moreover, the collection of experimental data is a need for the practical applications.

5. Conclusions

This paper investigates on the thermoelectric conversion performance of SiC ceramic structures on supersonic-vehicle nose tip under the conditions of different Mach numbers. The numerical analysis is performed with and without respect to the Thomson heat, respectively.

Results show that there is better thermoelectric performance at high Mach numbers. With the increased Mach numbers, both the output power and efficiency become higher because of growing temperature difference and heat flux attributed to the dramatically increased aero-heating. The maximum output power reaches 0.062 W at temperature difference of 670 K with M 4.5.

When the Thomson effect is considered, the thermoelectric performance is strongly weakened. There is over 50% of the generated power converting to Thomson heat due to the large temperature difference at each Mach number case. Notwithstanding, the thermoelectric conversion performance is continuously improved with the increase of Mach number. Moreover, the Thomson heat is possible to be eliminated by the optimization of Seebeck coefficient, which is a new research area of nanostructured materials and nanocomposites. Therefore, the thermoelectric technology used in aerodynamic heat recovery is very promising.

This research suggests a novel application of thermoelectric uniform structures acceptable for harvesting aerodynamic heat energy on supersonic vehicles, and also supplies fundamental data for limiting the aero-heating by thermoelectric technology.

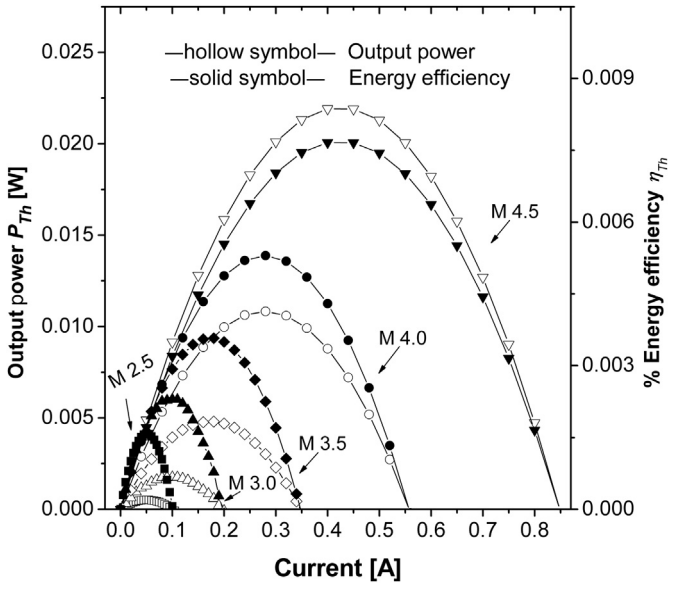

Fig. 13. Output power and energy efficiency versus current with respect to Thomson effect at different Mach numbers.

Acknowledgements

The authors would like to thank the support from Aid Program for Science and Technology Innovation Research Team in Higher Educational Institutions of Hunan Province and Aid Program for Innovative Group of National University of Defense Technology, and are grateful to colleagues of the Hypersonic Vehicles Research Centre, National University of Defense Technology, for the help and discussions on numerical solutions of the flow field and solid thermal conduction.

References

[1] J.-X. Liu, Z.-X. Hou, X.-Q. Chen, J.-T. Zhang, Experimental and numerical study on the aero-heating characteristics of blunted waverider, Appl. Therm. Eng. 51 (1–-2) (2013) 301–314.
[2] W. Peng, P.X. Jiang, Passive shock wave control in supersonic film cooling, J. Eng. Therm. 32 (10) (2011) 1731–1733.
[3] J. Sun, W.-Q. Liu, Investigation on integral model of heat-pipe-cooled leading edge of hypersonic vehicle, Acta Phys. Sin. 62 (7) (2013) 074401.
[4] Y.Q. Liu, P.X. Jiang, S.S. Jin, J.G. Sun, Transpiration cooling of a nose cone by various foreign gases, Int. J. Heat Mass. Transf. 53 (23–24) (2010) 5364–5372.
[5] H.B. Lu, W.Q. Liu, Numerical investigation on properties of attack angle for opposing jet thermal protection system, Chin. Phys. B 21 (8) (2012) 084401.
[6] H. Ye, X. Geng, The feasibility analysis of the application of TPV system in reentry, Sci. China Tech. Sci. 53 (2010) 3310–3315.
[7] J.-Y. Jang, Y.-C. Tsai, Optimization of thermoelectric generator module spacing and spreader thickness used in a waste heat recovery system, Appl. Therm. Eng. 51 (1–-2) (2013) 677–689.
[8] S.-K. Kim, B.-C. Won, S.H. Rhi, S.-H. Kim, J.-H. Yoo, J.-C. Jang, Thermoelectric power generation system for future hybrid vehicles using hot exhaust gas, J. Electron. Mater. 40 (5) (2011) 778–783.
[9] R.Y. Nuwayhid, D.M. Rowe, G. Min, Low cost stove-top thermoelectric generator for regions with unreliable electricity supply, Renew. Energy 28 (2) (2003) 205–222.
[10] G. Min, D.M. Rowe, Conversion efficiency of thermoelectric combustion systems, IEEE Trans. Energy Convers. 22 (2) (2007) 528–534.
[11] S.B. Riffat, X. Ma, Thermoelectrics: a review of present and potential applications, Appl. Therm. Eng. 23 (8) (2003) 913–935.
[12] X.Y. Han, J. Wang, H.F. Cheng, X. Xing, Numerical investigations of thermoelectric recovery of SiC ceramics for supersonic vehicles structures, in: 1st International Conference on Energy and Environmental Protection, Hohhot, 2012.
[13] C.C. Zhou, C.R. Zhang, H.F. Hu, Y.D. Zhang, Z.Y. Wang, Preparation process of C_f/SiC ceramic matrix composites, Rare Met. Mater. Eng. 36 (2007) 659–663.
[14] Y. Tang, J. Wang, X.D. Li, W.H. Li, H. Wang, X.Z. Wang, Thermal stability of polymer derived SiBNC ceramics, Ceram. Int. 35 (2009) 2871–2876.
[15] L.M. Ivanova, P.A. Aleksandrov, K.D. Demakov, Thermoelectric properties of vapor-grown polycrystalline cubic SiC, Inorg. Mater. 42 (11) (2006) 1205–1209.
[16] S. Fukuda, T. Kato, Y. Okamoto, H. Nakatsugawa, H. Kitagawa, S. Yamaguchi, Thermoelectric properties of single-crystalline SiC and dense sintered SiC for self-cooling devices, Jpn. J. Appl. Phys. 50 (3) (2011) 03130.
[17] Y. Yin, H. Chen, Y.J. He, Thermoelectric properties of Ti doped n-type SiC composites, Qinghua Daxue Xuebao 40 (2000) 5–7.
[18] D.C. Wilcox, Turbulence Modeling for CFD, DWC Industries, Canada, 1993.
[19] J.E. Bardina, P.G. Huang, Turbulence Modeling Validation, 1997. AIAA-97-2121.
[20] B.J. Van Leer, Towards the ultimate conservative difference scheme, V.A. second-order sequel to Godunov's method, J. Comput. Phys. 135 (1997) 229.
[21] J.C. Butcher, Stability property of implicit Runge–Kutta methods, BIT (Copenhagen) 15 (1975) 358–361.
[22] W.Q. Tao, Numerical Heat Transfer, second ed., Xi'an Jiaotong University Press, Xi'an, 2001 (in Chinese).

[23] G. Min, D.M. Rowe, K. Kontostavlakis, Thermoelectric figure-of-merit under large temperature differences, J. Phys. D 37 (2004) 1301–1304.
[24] M.J. Huang, R.H. Yen, A.B. Wang, The influence of the Thomson effect on the performance of thermoelectric cooler, Int. J. Heat Mass Transf. 48 (2005) 413–418.
[25] K. Hayashi, S. Aso, Y. Tani, Numerical Study of Thermal Protection System by Opposing Jet, 2005. AIAA 2005-188.
[26] X.Z. Cheng, Z.F. Xie, Y.C. Song, J.Y. Xiao, Structure and properties of polycarbosilane synthesized from polydimethylsilane under high pressure, J. Appl. Polym. Sci. 99 (2006) 1188–1194.
[27] A.J. Minnich, M.S. Dresselhaus, Z.F. Ren, G. Chen, Bulk nanostructured thermoelectric materials: current research and future prospects, Energy Environ. Sci. 2 (5) (2009) 466–479.